IEEE Access
Multidisciplinary | Rapid Review | Open Access Journal

Received November 10, 2019, accepted December 9, 2019, date of publication December 19, 2019,
date of current version December 31, 2019.

Digital Object Identifier 10.1109/ACCESS.2019.2960867

Passivity Based Damping Design for Grid-Connected Converter With Improved Stability

HUAIYUAN LIU[1], LEI LI[1], YUCHAO LIU[2], DIANGUO XU[1], (Fellow, IEEE), AND QIANG GAO[1]

[1]Electrical Engineering Department, Harbin Institute of Technology, Harbin 150001, China
[2]College of Automation, Harbin Engineering University, Harbin 150001, China

Corresponding author: Huaiyuan Liu (huaiyuan.liu@yahoo.com)

This work was supported in part by the National Natural Science Foundation of China under Grant 51720105008 and Grant 51807033.

ABSTRACT The impedance interactions between weak grid and LCL-filtered converter can bring severe harmonic resonance. Recently, frequency domain passivity theory has been applied to converter damping design. However, it is usually not easy to achieve full frequency passivity. What's more, traditional passivity based damping design is not enough for system robustness. This paper first proposes a relaxed passivity based active damping design for capacitor current feedback. Then the system stability under grid impedance variation is also analyzed. It has been found that the wide variation of grid impedance can decrease system stability margin. As a result, critical oscillation can even happen in the passive region of converter output admittance, causing power quality problems. In order to further improve system stability, this paper proposes an enhanced passivity based impedance shaping method, which is based on hybrid damping and combined active damping. Effects of damping methods and damping parameters are also investigated. A step by step damping design procedure is formulated, which is easy to implement. Simulation and experimental results validate the effectiveness of proposed method.

INDEX TERMS LCL filter, frequency domain passivity, hybrid damping, active damping.

I. INTRODUCTION

With the development of renewable energy system (RES), voltage source converters have been greatly accepted as the connection between RES and traditional power grid [1]–[5]. Grid-connected converters bring improved efficiency, but also cause unexpected problems [5]–[8].

Unlike traditional equipment, grid-connected converters utilize controllable high frequency semiconductor devices, which may inject plenty of switching harmonics to the power grid. Hence, filters are usually inserted between converters and grid to attenuate high order harmonics. Unlike the traditional simplest L filter, LCL filter can get better high frequency harmonic attenuation with a smaller inductance, reducing system weight and volume. However, LCL filter is a high order system. The resonance characteristics of LCL filter need to be solved for system stability [9]–[12].

The associate editor coordinating the review of this manuscript and approving it for publication was Yongle Wu.

Precious studies have been made in LCL filter stability analysis and resonance damping [12], but the effect of digital control delay is ignored [13], [14]. In addition, with the increase of RES, weak grid has become key factor to system stability. The grid impedance is non-negligible, which may interact with converter control loop, causing harmonic instability. What's worse, multiparallel converters may be interconnected though the point of common coupling (PCC). There also exist interactions among different converters. Even though single converter is stable, parallel converters system may also have harmonic resonance [5], [8]–[11], [15]–[17]. Hence, a practical tool is urgently needed for system analysis.

The impedance-based method was first applied in the design of DC-DC converters. Nowadays it has been extended to study the stability of grid connected converter system (DC-AC system). Converter and grid are modeled as the subsystems, and the system stability is determined by the impedance ratio of subsystems [5], [8]–[11], [15]–[19]. Compared with traditional state-space method, impedance-based

method does not need to build high order matrix. The modification in one subsystem does not affect the impedance model of other parts. The complex eigenproperties analysis of state matrix is also avoided, which simplifies process of system analysis. What's more, the impedance-based method can be treated as a design-oriented tool. System stability can be effectively achieved by impedance shaping [8], [18]–[20].

According to impedance-based method, frequency domain passivity can also be employed to guide the current controller and damping design [21]–[23]. Grid connected converter is passive if the output impedance has a non-negative real part, which means that the phase of impedance is limited to [-90°, 90°]. It is obvious that the grid impedance always has a non-negative real part. If the converter impedance is also passive, the impedance ratio would satisfy Nyquist stability criterion and system can keep stable [16], [21]. Passivity is a sufficient and unnecessary condition for stability [9], [23].

Several studies have been reported for passivity based resonance damping. Reference [11] proposes a passivity based design of passive damping for LCL filtered converter, however pure passive damping is often limited in application due to its damping loss and efficiency. Additional active damper is also considered to eliminate the non-passive region of converter output admittance [9]. The external active damper can behave as a virtual resistor in harmonic resonance frequency [5], [9]. Furthermore, a series LC filter can be used to reduce the power and voltage level [9]. Active damper can be plug-and-play and is not limited by grid connected converter controller bandwidth, but the expensive hardware cost may also not be acceptable. What's more, active damper is also affected by its own control delay and bandwidth [9]. A discrete derivative controller is proposed to reduce the non-passive region in [21], but this method cannot totally eliminate the non-passive region.

It can be found that full frequency passivity is usually not easy to be achieved in a relaxed and effective way [22], [23]. Complex damping design procedures are often needed. What's more, passivity is not enough to guarantee system robustness. Tradition passivity based damping design does not consider enough stability margin. Grid impedance wide variation can change the intersection point of grid impedance and converter output impedance, decreasing system phase margin, thus critical oscillation would still happen in passive region. So, in order to ensure the system stability under weak grid, traditional passivity damping method should be improved to get a satisfactory phase margin [18].

This paper mainly proposes an enhanced step by step damping method to ensure system stability margin under grid impedance variation. The impedance model of grid connected converter system is derived first. A simple capacitor current feedback active damping is also designed to minimize the non-passive region. Then this paper analyzes that grid impedance wide variation can greatly decrease stability margin, thus critical oscillation can also happen in the passive region, which is usually considered safe enough in the previous studies. The enhanced passivity based damping method is thus proposed to improve system stability, which is based on hybrid damping and combined active damping. A step by step design procedure is also formulated for easy implement.

The following part of this paper is organized as follows. Section II introduces system configuration and impedance modeling. Section III analyzes the converter non-passive region and discusses the passivity based active damping design. The performance under grid impedance variation is also investigated. The proposed enhanced damping design method are studied in Section IV. The simulation and experiment validations are shown in Section V. Section VI concludes this paper in the end.

II. IMPEDANCE MODELING OF GRID-CONNECTED CONVERTER

A. SYSTEM DESCRIPTION

The structure of LCL-filtered grid-connected converter system is shown in Fig. 1. LCL filter consists of L_1, L_2 and C. Z_g is the grid impedance. i_g is the grid current employed for the single loop current controller (shown as Fig. 2). The DC voltage is assumed as constant. Proportional plus resonant (PR) compensators in the stationary $\alpha\beta$ frame is used for current controller [24], [25]. Digital control can bring a computation delay and a ZOH delay. The total delay can be approximate to 1.5 sampling periods ($1.5T_s$) [5], [26]. The voltage source converter is interlinked to the weak grid through PCC.

Generally, converter has multi control loops and different loops may bring oscillations in different frequency ranges [15]. The grid synchronization (such as PLL) may bring negative resistor in low frequency. It has been proven

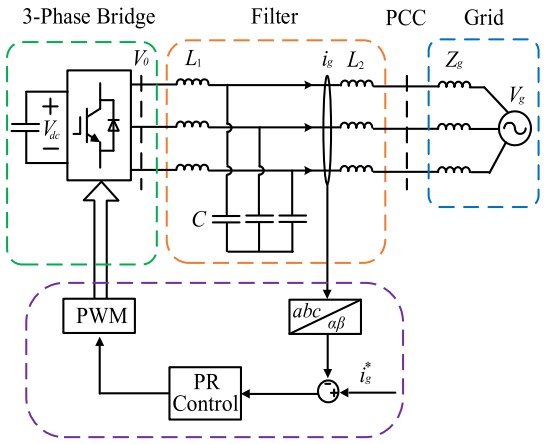

FIGURE 1. The structure of three phase LCL-filtered grid-connected converter.

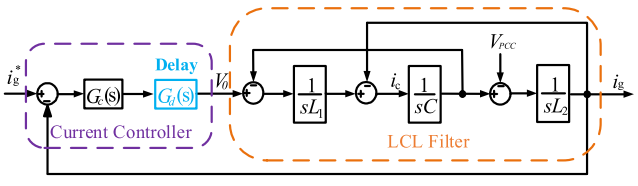

FIGURE 2. Block diagram of single current control loop for converter.

in [27] that the frequency range of negative resistor is only affected by PLL bandwidth. It has also been noted that reducing PLL bandwidth can reduce the potential unstable frequency range, eliminating the low frequency oscillations [27]. In order to simplify the system model, the PLL bandwidth is designed much lower than the current loop bandwidth and filter resonance frequency, therefore its effect on system stability can be ignored [5], [27], [28].

B. IMPEDANCE MODELING OF GRID-CONNECTED CONVERTER SYSTEM

Impedance model for LCL-filtered grid-connected converter system would be derived here first. For the voltage source converter shown in Fig. 1 and Fig. 2, it can be equivalent to an ideal current source and a parallel output impedance (shown in Fig. 3, admittance expression is used for convenience) [5]. By using equivalent transformation, the simplified equivalent block diagram is illustrated in Fig. 4 [24]. The expressions of G_{x1} and G_{x2} are shown in (1) and (2). It should be noted that G_{x1} and G_{x2} are just the equivalent result of the system transformation, there is no accurate physical meaning in practice. G_c represents the current controller and G_d is the 1.5 period delay.

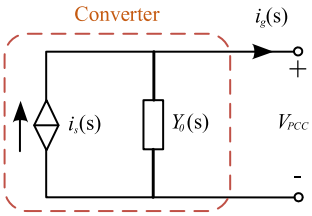

FIGURE 3. Norton equivalent circuit of converter with single current control loop.

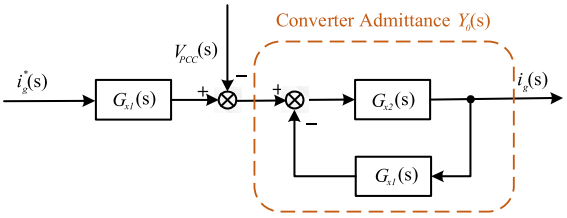

FIGURE 4. Simplified equivalent diagram of single current control loop in Fig. 2.

The transfer function for G_c and G_d are shown in (3), K_p and K_r are the current controller gain and ω_f is the fundamental frequency. In fact, since the resonant controller mainly affects the fundamental frequency, the current controller can be simplified as a proportional part in stability analysis [16].

In fact, the whole system is not just an ideal scalar system. There also exists coupling interaction in converter impedance model. Therefore, the whole system is a multi-in-multi-out (MIMO) system. For the PR current controller in the stationary frame, if PLL is neglected, the system can be considered as decoupled single-in-single-out (SISO) systems [5], [16], [24]. For the PI current controller in dq frame, if the grid connected converter works in the high power factor, the system can also be considered as decoupled SISO systems [29].

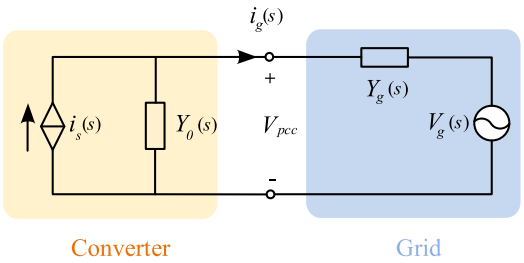

FIGURE 5. Impedance model of grid connected converter system.

$$G_{x1} = \frac{G_d G_c Z_C}{Z_{L1} + Z_C} \tag{1}$$

$$G_{x2} = \frac{Z_{L1} + Z_C}{Z_{L1}Z_{L2} + (Z_{L1} + Z_{L2})Z_C} \tag{2}$$

$$G_c = K_p + \frac{K_r s}{s^2 + \omega_f^2} \qquad G_d = e^{-1.5T_s s} \tag{3}$$

The converter output admittance Y_0 can be derived as (4) and (5). The grid current i_g in Fig. 3 can be shown as (6). Furthermore, Fig. 5 illustrates the whole impedance model of grid-connected converter system, in which weak grid is modeled as a voltage source V_g in series with the grid admittance Y_g.

$$Y_0 = \frac{G_{x2}}{1 + G_{x1}G_{x2}} = \frac{Z_{L1} + Z_C}{Z_{L1}Z_{L2} + (Z_{L1} + Z_{L2})Z_C + G_d G_c Z_C} \tag{4}$$

$$Y_0 = \frac{1 + s^2 L_1 C}{s^3 L_1 L_2 C + sL_1 + sL_2 + G_d G_c} \tag{5}$$

$$i_g = i_s - Y_0 V_{PCC} \qquad i_s = \frac{G_{x1}G_{x2}}{1 + G_{x1}G_{x2}} i_g^* \tag{6}$$

For Fig. 5, the grid current can be expressed as (7). It can be seen that, if the converter is designed to be stable in ideal grid, system stability of (7) would be determined by the right part. The open loop transfer function for the right part can be shown in (8), which is the admittance ration between converter and grid [30].

$$i_g = \frac{Y_g}{Y_0 + Y_g} i_s - \frac{Y_0 Y_g}{Y_0 + Y_g} V_g = (i_s - Y_0 V_g) \frac{1}{1 + Y_0/Y_g} \tag{7}$$

$$T_m = \frac{Y_0}{Y_g} \tag{8}$$

III. PASSIVITY BASED DAMPING DESIGN

A. NON-PASSIVE REGION FOR CONVERTER

Frequency domain passivity concept has been mentioned in [16], [18]. Admittance Y is defined passive only if it has a non-negative real part. The phase angle of a passive admittance is between [-90°, 90°] (shown in Fig. 6). Since grid admittance consists of passive components, its real part

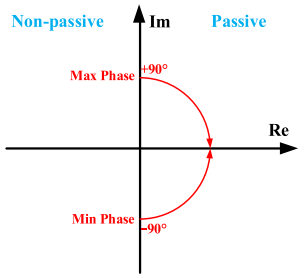

FIGURE 6. Frequency domain passivity theory.

is usually non-negative. In other words, the grid always has a passive admittance. If the converter output admittance is also passive, the phase difference at the grid and converter admittance intersection point will be less than 180°. That is, there is a positive phase margin and system would be stable. Passivity can be defined as a grid code in RES [18].

In order to derive the converter non-passive region, the real part of (4) and (5) should be derived first [9], [16], which is shown in (9)–(11). According to (9), it can be found that the non-passive region is between $[f_{LC}, f_s/6]$, and f_{LC} is resonance frequency for L_1 and C. System parameters are shown in Table 1. The Bode plots in Fig. 7 validate the derivation.

In weak grid, if the intersection point of converter and grid admittance is located in the non-passive region (shown as Fig. 7), the phase difference would beyond 180°. According to stability criterion, the phase margin is negative, and the

TABLE 1. System parameters.

Symbol	Name of parameters	Value
Z_g	Grid impedance	7.2mH
L_2	Grid-side inductor	1.8mH
C	Filter capacitor	6uF
L_1	Converter-side inductor	2.7mH
K_p	Proportional gain	12
K_r	Resonant gain	900
T_s	Sampling Time	1e-4s
f_s	Switching Frequency	10K
ω_f	Fundamental frequency	50Hz

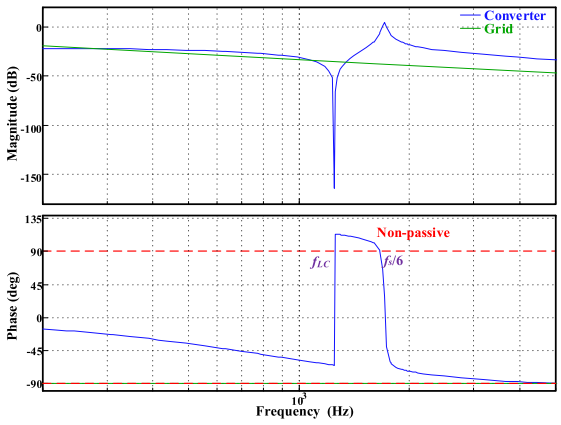

FIGURE 7. Passive and non-passive regions for converter output admittance without damping (Z_g = 7.2mH).

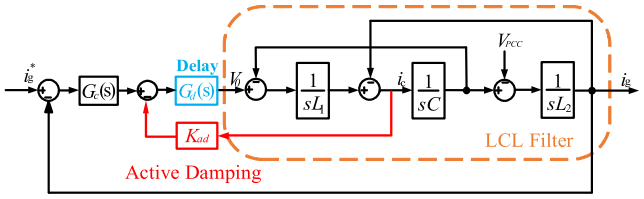

FIGURE 8. Control block diagram of capacitor-current-feedback active damping for converter.

impedance interaction between converter and grid makes the whole system unstable.

$$\mathrm{Re} = \frac{G_c \cos(1.5\omega T_s)(1-\omega^2 L_1 C)}{A^2 + B^2} \tag{9}$$

$$A = G_c \sin(1.5\omega T_s) + \omega(\omega^2 L_1 L_2 C - L_1 - L_2) \tag{10}$$

$$B = G_c \cos(1.5\omega T_s) \tag{11}$$

B. PASSIVITY BASED ACTIVE DAMPING DESIGN

Since unexpected harmonic resonance would happen in weak grid, additional damping should be added to increase system freedom and improve system stability. It is noted that non-passive region is the potential stability threat to system operation, thus the main designing objective for damping is to minimize the non-passive region.

Active damping method is often preferred for a better efficiency [12], [31]. Since capacitor current feedback is one of the most popular active damping, it is chosen here as the relaxed method to achieve passivity. It can be equivalent to an impedance in parallel with the filter capacitor [13]. The equivalent damping impedance can help to reduce the converter non-passive region. Control block diagram of capacitor current feedback active damping is shown in Fig. 8, and K_{ad} is the feedback gain. The equivalent transformation for converter with active damping is the same as Fig. 4. The output admittance of converter with capacitor current feedback active damping can be derived in (4) and (12)-(15).

The passivity based active damping design can be achieved by tuning the feedback gain K_{ad}. The Bode plots are shown in Fig. 9 (not all of the Bode plots are shown here for simplicity). According to Fig. 9, it can be found that K_{ad} can be chosen as 5 for a negligible non-passive region. After applying passivity based active damping, the system would recover stable.

$$G_{x1} = \frac{G_d G_c Z_C}{Z_{L1} + Z_C + K_{ad} G_d} \tag{12}$$

$$G_{x2} = \frac{Z_{L1} + Z_C + K_{ad} G_d}{Z_{L1} Z_{L2} + (Z_{L1} + Z_{L2}) Z_C + K_{ad} G_d Z_{L2}} \tag{13}$$

$$Y_0 = \frac{Z_{L1} + Z_C + K_{ad} G_d}{Z_{L1} Z_{L2} + (Z_{L1} + Z_{L2}) Z_C + K_{ad} G_d Z_{L2} + G_d G_c Z_C} \tag{14}$$

$$Y_0 = \frac{1 + s^2 L_1 C + s C K_{ad} G_d}{s^3 L_1 L_2 C + s L_1 + s L_2 + G_d G_c + K_{ad} G_d s^2 L_2 C} \tag{15}$$

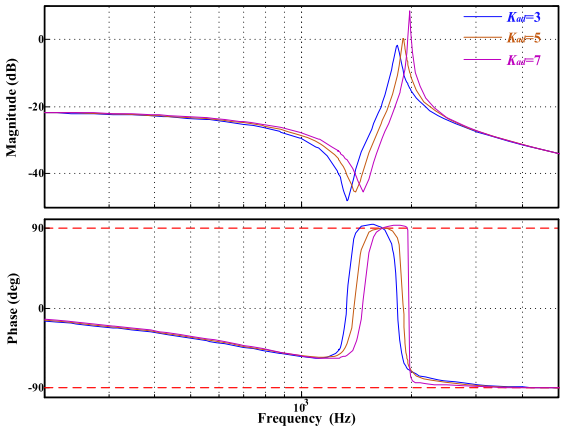

FIGURE 9. Converter output admittance with the tuning of capacitor current feedback gain $K_{ad} = 3, 5, 7$.

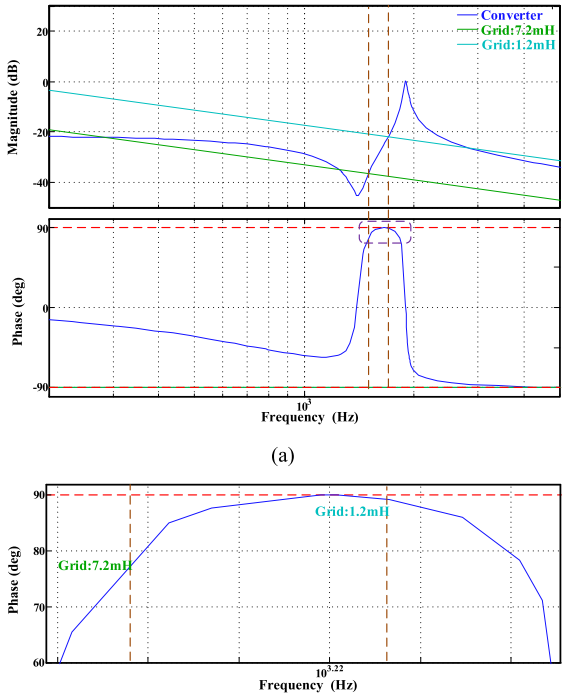

FIGURE 10. (a) Bode plots for converter and grid under grid impedance variation. $K_{ad} = 5$ (b) Zoomed view for stability margin.

C. PERFORMANCE UNDER GRID IMPEDANCE VARIATION

For the grid-connected converter shown in Fig. 5 and Fig. 10, even though converter output admittance is passive, critical oscillation may still happen if there is not enough phase margin. This phenomenon is caused by the wide variation of grid impedance.

For example, if grid impedance decreases to 1.2mH, although the intersection point falls into passive region (shown as Fig. 10), phase margin is very small (only 0.5°). There would be underdamped harmonic distortion in grid current (will be shown in Section V) [18]. What's more, considering the converter parameter variation, situation can

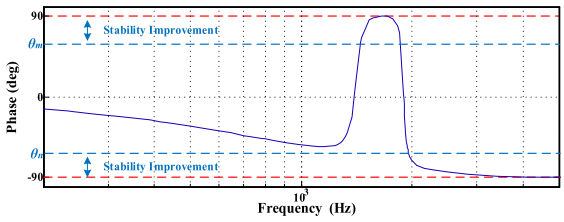

FIGURE 11. Restricted phase limit for stability improvement.

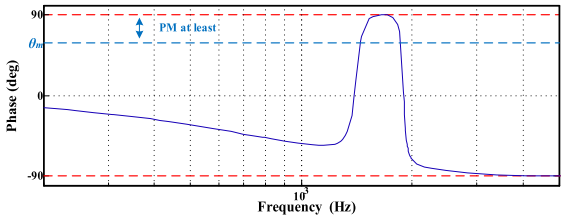

FIGURE 12. Enhanced passivity based damping method with improved stability.

be even worse. It can be seen that passivity is not enough to system robustness. Stability margin must be improved to guarantee the output power quality, which can be achieved by additional damping method.

IV. ENHANCED PASSIVITY BASED DAMPING DESIGN METHOD

In order to improve the system stability, traditional passivity based damping method should be modified to guarantee enough phase margin. A more restricted phase limit should be required, which can be set as $[\theta_n, \theta_m]$, shown in Fig. 11. Since most of the grid impedances are inductive, the minimum phase for converter output admittance can be set to -90° (shown in Fig. 12). A phase margin of at least 90°-θ_m can be obtained in full frequency even with the wide variation of grid impedance [18]. The enhanced passivity based damping design method and its performance under grid impedance variations would be discussed later.

A. STABILITY MARGIN IMPROVEMENT BY HYBRID DAMPING

The enhanced passivity based damping can be realized by employing additional series resistor, which is also called hybrid damping method, shown as Fig. 13. The control block diagram of hybrid damping is shown in Fig. 14. Compared with pure passive damping, the required damping resistor can be reduced by active damping [32]. The converter output admittance for hybrid damping is also derived as (12)–(14), but the impedance of capacitor should be considered as (16).

$$Z_c = R_d + \frac{1}{sC} \tag{16}$$

By tuning damping resistor, Bode plots for hybrid damping are shown in Fig. 15. From Fig. 15, it can be found the phase margin is improved with the larger damping resistor, but the damping loss is also increased [11], [32]. This is because the

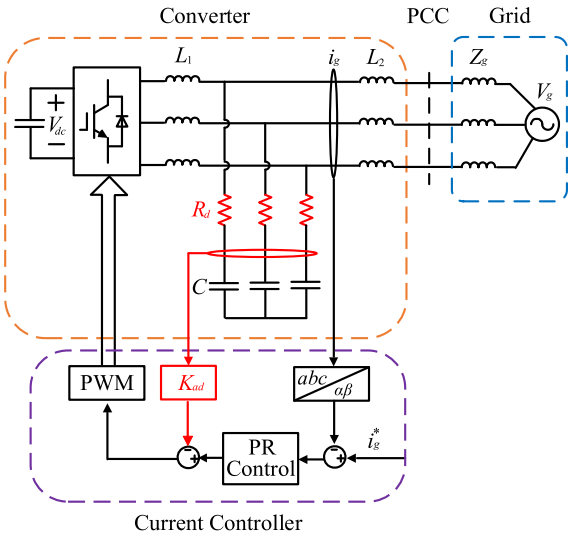

FIGURE 13. The structure of grid connected converter with hybrid damping.

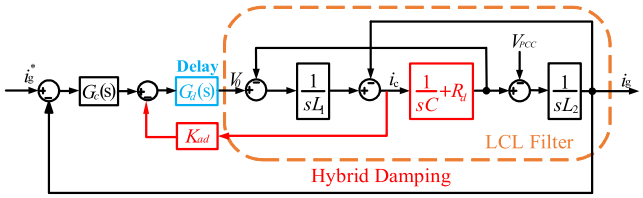

FIGURE 14. Control block diagram of grid connected converter with hybrid damping.

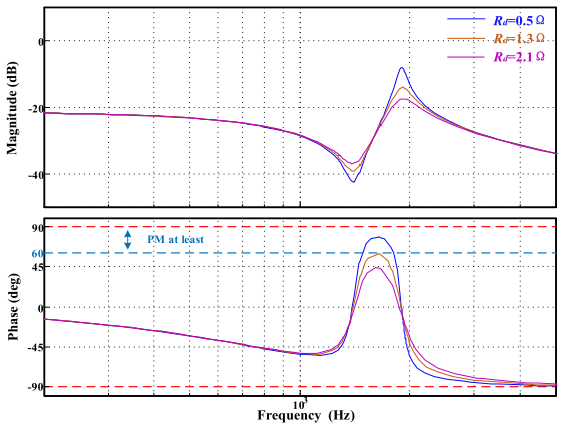

FIGURE 15. Bode plots for converter output admittance with tuning of damping resistor R_d = 0.5, 1.3, 2.1Ω.

damping loss mainly consists of low frequency loss and high frequency loss [33]. According to [33], in the low frequency, the current through damping resistor is mainly determined by the filter capacitor while in high frequency the current is mainly determined by the filter inductor. Reference [33] also proves that the damping loss is proportional to the damping resistor.

About 1.3Ω damping resistor is needed for 30° phase margin and more than 2Ω damping resistor is needed for 45° phase margin. It should be noted that the additional damping resistor is not affected by control delay, which means that no additional non-passive region would be brought.

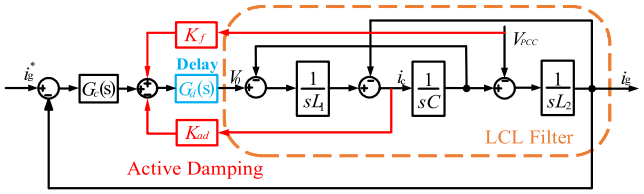

FIGURE 16. Control block diagram of grid voltage feedforward and capacitor current feedback active damping.

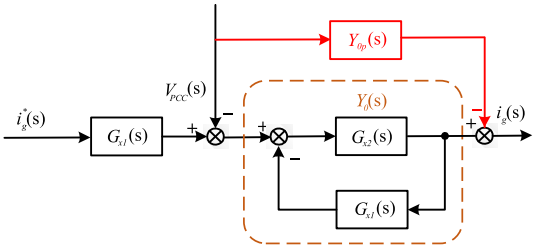

FIGURE 17. Equivalent transformation of grid voltage feedforward active damping.

B. STABILITY MARGIN IMPROVEMENT BY COMBINED ACTIVE DAMPING

Even though Hybrid damping does not introduce non-passive region, the damping loss is not expected in most cases. The enhanced passivity based damping can also be achieved by combined active damping method.

Grid voltage feedforward can be first employed in combined active damping to bring additional control freedom and enhance damping effect. Since PCC voltage is usually sampled for phase lock loop, no additional sensor is required. The control block diagram and equivalent transformation block for grid voltage feedforward is shown in Fig 16 and Fig 17, while K_f is feedforward gain. According to Fig 17, it can be equivalent to a virtual admittance Y_{0p} in parallel with original converter admittance Y_0 (shown in Fig. 17) [34]. Thus, the whole output admittance Y_1 will be reshaped. Y_{0p} can be derived as (17) and Y_1 can be derived as (18) – (20).

By tuning the voltage feedforward parameter, the Bode plots for converter output admittance is shown in Fig. 18. It can be seen that, in order to ensure enough phase margin, a larger feedforward gain is usually needed. However, with the increase of K_f, a non-passive region beyond -90° is also appears in mid-frequency. So K_f is set to 0.35 for a phase margin of 30° as a trade-off.

$$Y_{0p} = -K_f \frac{G_{x1}}{G_c} Y_0 \tag{17}$$

$$Y_1 = Y_{0p} + Y_0 \tag{18}$$

$$\frac{Y_1}{Y_0} = 1 - K_f \frac{G_{x1}}{G_c} \tag{19}$$

$$Y_1 = = \frac{Z_{L_1} + Z_C + G_d K_{ad} - K_f G_d Z_C}{G_c G_d Z_C + Z_{L_1} Z_{L_2} + (Z_{L_1} + Z_{L_2}) Z_C + G_c K_{ad} Z_{L_2}} \tag{20}$$

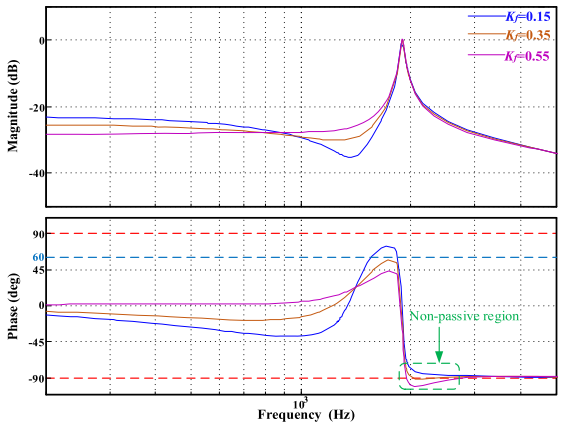

(a)

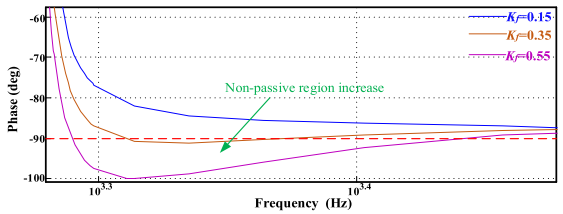

(b)

FIGURE 18. (a) Bode plots for converter output admittance with tuning of feedforward gain $K_f = 0.15, 0.35, 0.55$. (b) Zoomed view for non-passive region.

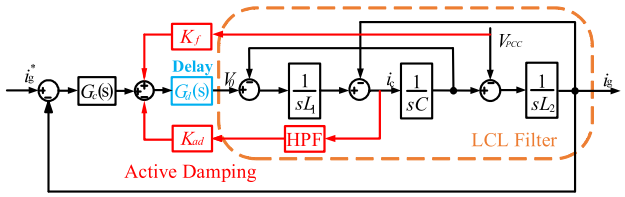

FIGURE 19. Control block diagram of combined active damping for converter.

In order to further mitigate the non-passive region brought by PCC voltage feedforward. High pass filter (HPF) can be added in capacitor feedback active damping [13]. The transfer function of high pass filter can be shown in (21). The whole control block of combined active damping is shown as Fig. 19. The cutoff frequency ω_f is chosen as 7500rad/s, Bode plot after applying high pass filter is shown in Fig. 20. It can be found that after applying the high pass filter, not only the additional non-passive region is eliminated, but the stability margin is also improved greatly.

$$G_{HPF} = \frac{s}{s + \omega_f} \tag{21}$$

C. STEP BY STEP DAMPING DESIGN FOR ENHANCED PASSIVITY

A step by step damping design procedure can be formulated as fellows. (1) Design the capacitor feedback parameter K_{ad} to achieve frequency passivity. (2) Design the damping resistor R_d (hybrid damping) or voltage feedforward parameter

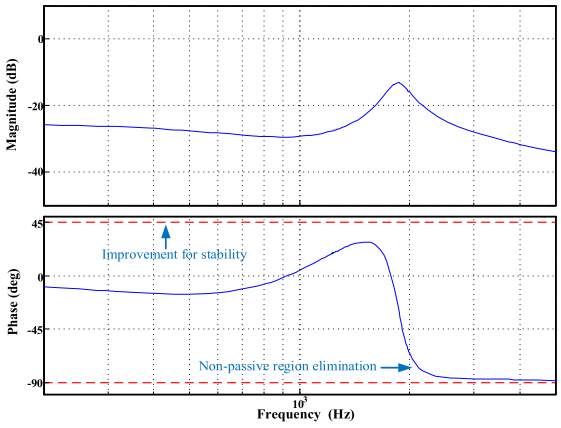

FIGURE 20. Bode plot for converter output admittance with combined active damping.

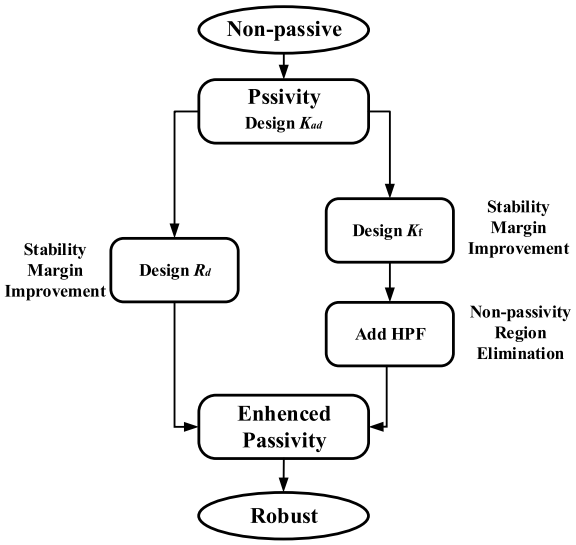

FIGURE 21. Step by step design procedure for enhanced passivity (hybrid damping in the left and combined active damping in the right).

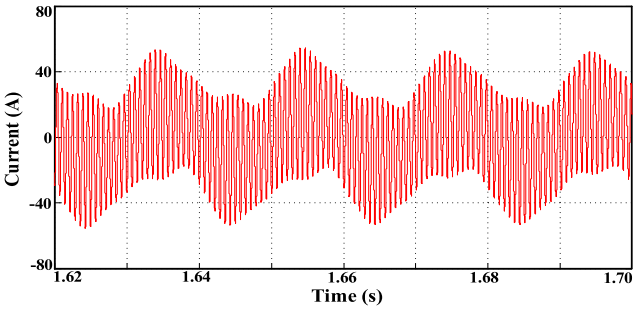

FIGURE 22. Simulated grid current without damping in weak grid, $Z_g = 7.2$mH.

K_f (combined active damping) to improve stability margin (3) Add high pass filter in capacitor current feedback to eliminate the additional non-passive region bought by PCC voltage feedforward (combined active damping). Since only one parameter is considered in every step, it is quite easy to implement. The formulated damping design procedure can be shown in Fig. 21.

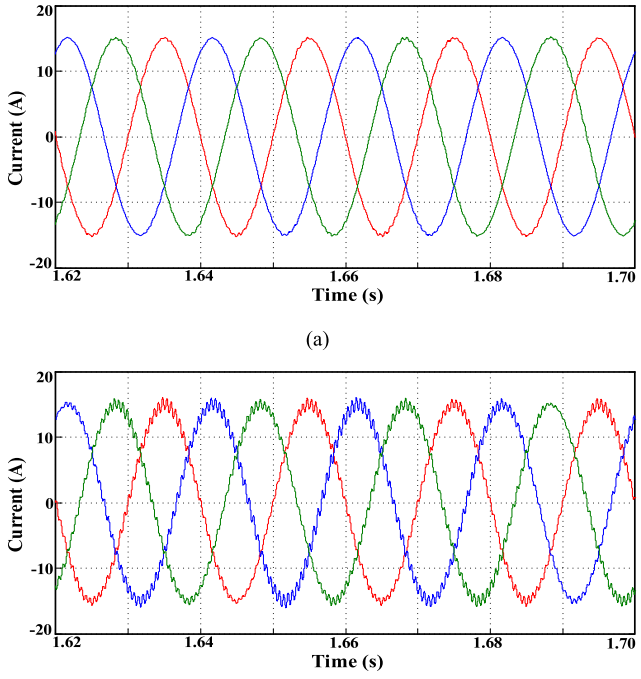

FIGURE 23. Simulated grid current with passivity based damping in weak grid, (a) $Z_g = 7.2$mH (b) $Z_g = 1.2$mH.

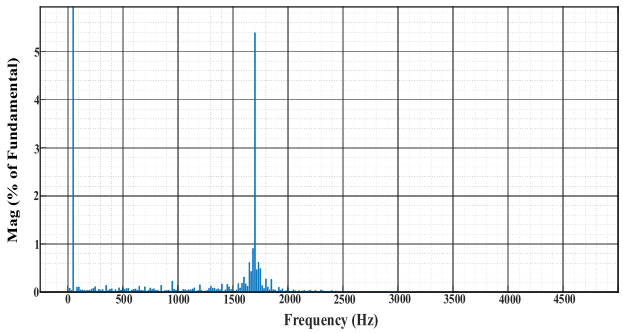

FIGURE 24. FFT analysis for simulated grid current with passivity based damping in weak grid, $Z_g = 1.2$mH (critical oscillation).

V. SIMULATION AND EXPERIMENT RESULTS

In order to validate the stability analysis and proposed impedance shaping method in Section III and IV, a time domain simulation model for grid connected converter system is built in Matlab/Simulink. The system configuration and parameters have been shown in Section II and III. A two level LCL filtered voltage source converter platform is also built for experimental verification.

A. SIMULATION RESULTS

The simulated grid current for converter without any damping in weak grid ($Z_g = 7.2$mH) is shown in Fig. 22, for the sake of a clear view, only single phase resonance current is given (since the current cannot amplify unlimitedly in practice, a very small damping resistance is added in simulation). According to Fig. 7, since the intersection point falls in non-passive region, the phase margin is negative and system is unstable. The simulation result agrees with the Bode plot analysis.

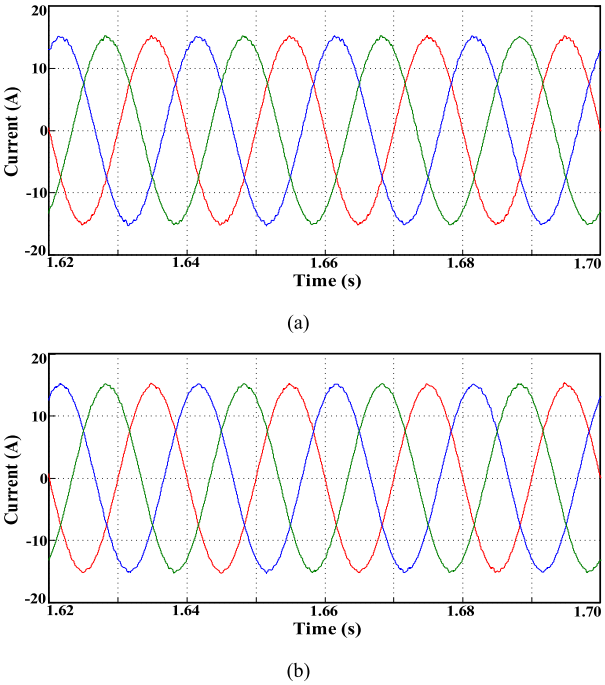

FIGURE 25. Simulated grid current with enhanced passivity based damping design (a) hybrid damping in weak grid, $Z_g = 1.2$mH (b) with combined active damping in weak grid, $Z_g = 1.2$mH.

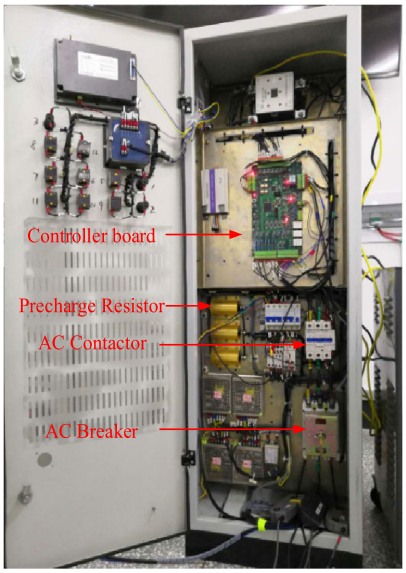

FIGURE 26. The photograph of experimental prototype.

Fig. 23(a) shows the simulated grid currents with capacitor current feedback active damping ($Z_g = 7.2$mH). With the help of passivity based damping design, non-passive region has been eliminated. The stable simulated current verifies the analysis in Section III B and C.

Corresponding to the grid currents in Fig 23(b), it has been found that, after the grid impedance varies to 1.2mH, the reduced phase margin deteriorates system stability.

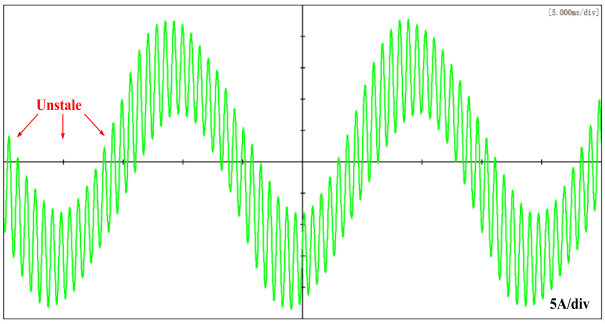

FIGURE 27. Experimental grid current without damping in weak grid, Zg = 7.2mH.

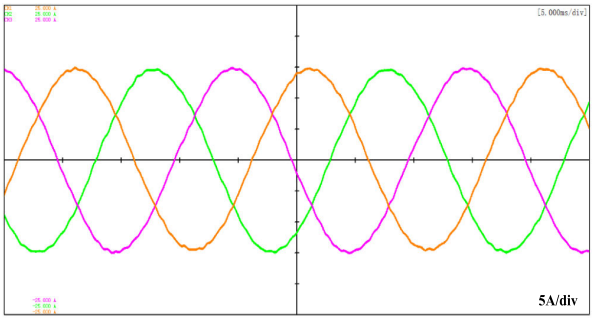

(a)

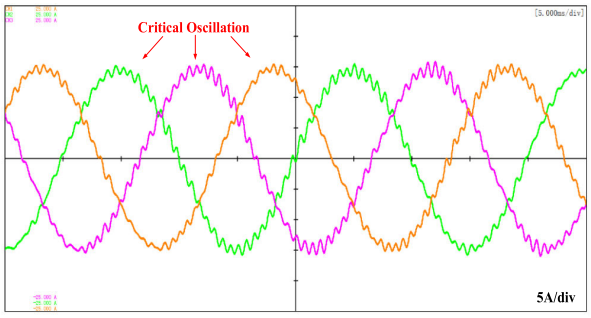

(b)

FIGURE 28. Experimental grid current with passivity based active damping in weak grid, (a) $Z_g = 7.2$mH (b) $Z_g = 1.2$mH.

A critical oscillation could be found in the grid current, which validates the analysis in Section III C. From the Bode plots in Fig. 10(b), the critical oscillation frequency is near 1690Hz. The FFT analysis for simulated current in Fig. 23(b) is shown as Fig. 24. It can be found that the simulated critical oscillation frequency is about 1700Hz, which matches the frequency domain analysis.

After applying the proposed enhanced damping design, the grid current is shown as Fig 25 (a) and (b), while (a) uses hybrid damping and (b) uses combined active damping. Compared with Fig 23(b), the simulation results show that the proposed enhanced damping method can improve stability margin effectively.

B. EXPERIMENT RESULT

A two level LCL filtered voltage source converter has been built to further verify the proposed damping method. The control algorithms are implemented in a Digital Signal Processor

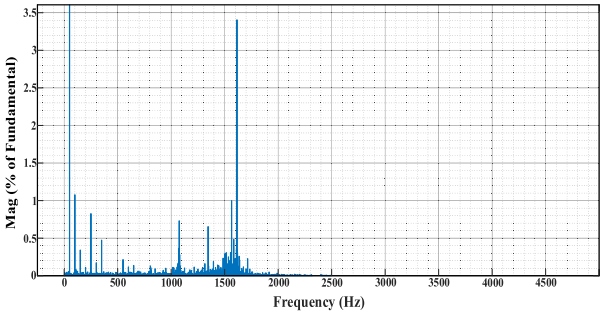

FIGURE 29. FFT analysis for experimental grid current with passivity based damping in weak grid, $Z_g = 1.2$mH (critical oscillation).

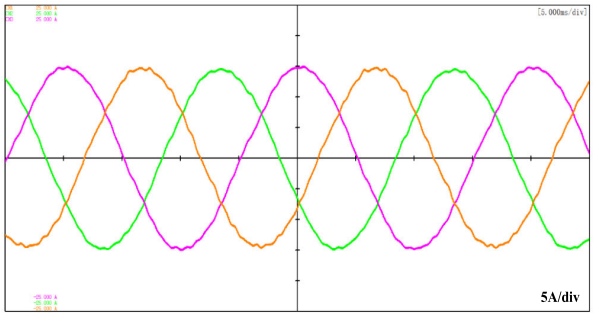

(a)

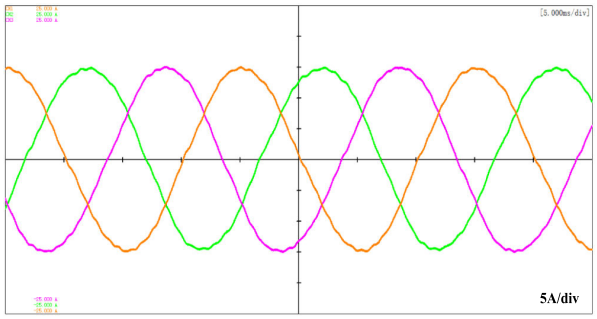

(b)

FIGURE 30. Experimental grid current (a) with enhanced passivity based damping (hybrid damping) in weak grid, $Z_g = 1.2$mH (b) with enhanced passivity based damping (combined active damping) in weak grid, $Z_g = 1.2$mH.

(TMS320F28335). The weak grid is emulated by AC programmable source and grid impedance inductance. The photograph of experimental prototype is shown in Fig. 26. The grid current is recorded by scope Yokogawa DL850E.

The experimental grid current in weak grid ($Z_g = 7.2$mH) without any damping is shown in Fig. 27 (for the sake of a clear view, only single phase resonance current is given here), it can be found that since the phase margin is negative, the system is unstable, an obvious resonance occurs.

After applying the passivity based capacitor current feedback active damping, the system recover stable (shown in Fig. 28(a)), which validates the Bode plots in Section III B and the simulation results in Fig. 23(a). It can be found that the passivity based damping can eliminate the harmonic resonance effectively.

The experimental grid current for passivity based damping design under 1.2mH grid impedance is shown in Fig. 28(b).

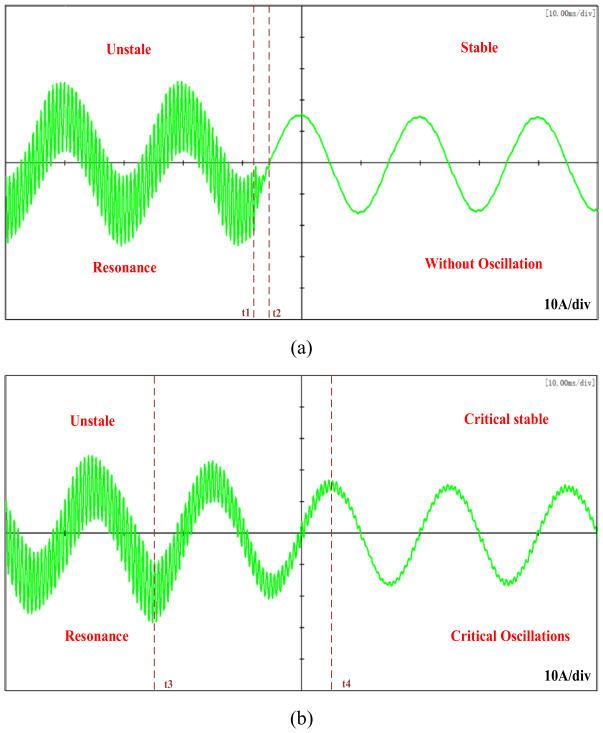

FIGURE 31. **Transitions for introducing additional damping, $Z_g = 1.2$mH (a) enhanced passivity based damping (b) traditional passivity based active damping.**

A critical oscillation can be observed. The experiment results agree to the Bode plots in Section III C and simulation result in Fig. 23(b). It can be found that, grid impedance variation can decrease system stability margin and passivity is not enough for system robustness.

The FFT analysis result for experimental current in Fig. 28(b) is shown as Fig. 29. It can be found that the experimental oscillation frequency is about 1600-1700Hz, which also validates the theoretical analysis.

The grid currents after applying hybrid damping and combined active damping are illustrated in Fig. 30(a) and Fig. 30(b). Compared with Fig. 28(b), it can be found that the critical oscillation is well damped. The experimental results prove the effectiveness of enhanced passivity based damping method.

The transitions after introducing additional damping are shown as Fig. 31. The dynamic experimental result for proposed enhanced passivity based damping (Combined active damping is chosen here for example) method is given in Fig. 31 (a), the additional damping is introduced in t_1, and system recover stable in t_2. The dynamic experimental result for traditional passivity based damping is given in Fig. 31(b). The damping is implemented in t_3 and system recover critical stable in t_4. It can be found that since the proposed damping method has improved stability margin, system can recover stable in a faster way. Except for the critical oscillation, the traditional passivity based damping method also needs a slower transition. The dynamic experimental results also validate the effectiveness of proposed method.

VI. CONCLUSION

The non-passive region of converter output impedance can cause harmonic instability in weak grid. In this paper, the impedance model of grid connected converter system is derived first. The damping parameter of capacitor current feedback is then designed to achieve a passive output impedance. However, passivity is not enough for system stability. This paper analyzes the relationship between stability margin and power quality, pointing that grid impedance variation can decrease phase margin, causing harmonic distortion of output current. In this paper, an enhanced passivity based damping method is proposed to improve system stability. Hybrid damping and combined active damping are employed. High pass filter is also added to eliminate the non-passive region brought by grid voltage feedforward in combined active damping. A step by step design procedure is also formulated. The proposed method can ensure a phase margin under grid impedance variation and converter parallel. Simulation and experiment results show the validation and effectiveness of proposed damping method under grid impedance variation.

REFERENCES

[1] J. Rocabert, A. Luna, F. Blaabjerg, and P. Rodriguez, "Control of power converters in AC microgrids," *IEEE Trans. Power Electron.*, vol. 27, no. 11, pp. 4734–4749, Nov. 2012.

[2] Y. Gu, N. Bottrell, and T. C. Green, "Reduced-order models for representing converters in power system studies," *IEEE Trans. Power Electron.*, vol. 33, no. 4, pp. 3644–3654, Apr. 2018.

[3] W. Li, Y. Gu, H. Luo, W. Cui, X. He, and C. Xia, "Topology review and derivation methodology of single-phase transformerless photovoltaic inverters for leakage current suppression," *IEEE Trans. Ind. Electron.*, vol. 62, no. 7, pp. 4537–4551, Jul. 2015.

[4] Y. Gu, Y. Li, H.-J. Yoo, T.-T. Nguyen, X. Xiang, H.-M. Kim, A. Junyent-Ferre, and T. C. Green, "Transfverter: Imbuing transformer-like properties in an interlink converter for robust control of a hybrid AC–DC microgrid," *IEEE Trans. Power Electron.*, vol. 34, no. 11, pp. 11332–11341, Nov. 2019, doi: 10.1109/TPEL.2019.2897460.

[5] X. Wang, F. Blaabjerg, M. Liserre, Z. Chen, J. He, and Y. Li, "An active damper for stabilizing power-electronics-based AC systems," *IEEE Trans. Power Electron.*, vol. 29, no. 7, pp. 3318–3329, Jul. 2014.

[6] R. N. Beres, X. Wang, M. Liserre, F. Blaabjerg, and C. L. Bak, "A review of passive power filters for three-phase grid-connected voltage-source converters," *IEEE Trans. J. Emerg. Sel. Topics Power Electron.*, vol. 4, no. 1, pp. 54–69, Mar. 2016.

[7] Z. Shuai, D. Liu, J. Shen, C. Tu, Y. Cheng, and A. Luo, "Series and parallel resonance problem of wideband frequency harmonic and its elimination strategy," *IEEE Trans. Power Electron.*, vol. 29, no. 4, pp. 1941–1952, Apr. 2014.

[8] X. Wang, F. Blaabjerg, and W. Wu, "Modeling and analysis of harmonic stability in an AC power-electronics-based power system," *IEEE Trans. Power Electron.*, vol. 29, no. 12, pp. 6421–6432, Dec. 2014.

[9] H. Bai, X. Wang, P. C. Loh, and F. Blaabjerg, "Passivity enhancement of grid-tied converters by series LC-filtered active damper," *IEEE Trans. Ind. Electron.*, vol. 64, no. 1, pp. 369–379, Jan. 2017.

[10] H. Bai, X. Wang, and F. Blaabjerg, "Passivity enhancement in renewable energy source based power plant with paralleled grid-connected VSIs," *IEEE Trans. Ind. Appl.*, vol. 53, no. 4, pp. 3793–3802, Jul./Aug. 2017.

[11] X. Wang, R. Beres, F. Blaabjerg, and P. Loh, "Passivity-based design of passive damping for LCL-filtered voltage source converters," in *Proc. IEEE Energy Convers. Congr. Expo. (ECCE)*, Montreal, QC, Canada, Sep. 2015, pp. 3718–3725.

[12] C. Bao, X. Ruan, X. Wang, W. Li, D. Pan, and K. Weng, "Step-by-step controller design for LCL-type grid-connected inverter with capacitor–current-feedback active-damping," *IEEE Trans. Power Electron.*, vol. 29, no. 3, pp. 1239–1253, Mar. 2014.

[13] X. Wang, F. Blaabjerg, and P. C. Loh, "Virtual RC damping of LCL-filtered voltage source converters with extended selective harmonic compensation," *IEEE Trans. Power Electron.*, vol. 30, no. 9, pp. 4726–4737, Sep. 2015.
[14] Z. Xin, P. C. Loh, X. Wang, F. Blaabjerg, and Y. Tang, "Highly accurate derivatives for LCL-filtered grid converter with capacitor voltage active damping," *IEEE Trans. Power Electron.*, vol. 31, no. 5, pp. 3612–3625, May 2016.
[15] X. Wang, L. Harnefors, and F. Blaabjerg, "Unified impedance model of grid-connected voltage-source converters," *IEEE Trans. Power Electron.*, vol. 33, no. 2, pp. 1775–1787, Feb. 2018.
[16] C. Yoon, H. Bai, R. N. Beres, X. Wang, C. L. Bak, and F. Blaabjerg, "Harmonic stability assessment for multiparalleled, grid-connected inverters," *IEEE Trans. Sustain. Energy*, vol. 7, no. 4, pp. 1388–1397, Oct. 2016.
[17] F. Wang, J. L. Duarte, M. A. M. Hendrix, and P. F. Ribeiro, "Modeling and analysis of grid harmonic distortion impact of aggregated DG inverters," *IEEE Trans. Power Electron.*, vol. 26, no. 3, pp. 786–797, Mar. 2011.
[18] Y. Gu, W. Li, and X. He, "Passivity-based control of DC microgrid for self-disciplined stabilization," *IEEE Trans. Power Syst.*, vol. 30, no. 5, pp. 2623–2632, Sep. 2015.
[19] J. Sun, "Small-signal methods for AC distributed power systems–a review," *IEEE Trans. Power Electron.*, vol. 24, no. 11, pp. 2545–2554, Nov. 2009.
[20] A. Adib, B. Mirafzal, X. Wang, and F. Blaabjerg, "On stability of voltage source inverters in weak grids," *IEEE Access*, vol. 6, pp. 4427–4439, 2018.
[21] X. Wang, F. Blaabjerg, and P. C. Loh, "Passivity-based stability analysis and damping injection for multiparalleled VSCs with LCL filters," *IEEE Trans. Power Electron.*, vol. 32, no. 11, pp. 8922–8935, Nov. 2017.
[22] L. Harnefors, X. Wang, A. G. Yepes, and F. Blaabjerg, "Passivity-based stability assessment of grid-connected VSCs-an overview," *IEEE J. Emerg. Sel. Topics Power Electron.*, vol. 4, no. 1, pp. 116–125, Mar. 2016.
[23] L. Harnefors, R. Finger, X. Wang, H. Bai, and F. Blaabjerg, "VSC input-admittance modeling and analysis above the Nyquist frequency for passivity-based stability assessment," *IEEE Trans. Ind. Electron.*, vol. 64, no. 8, pp. 6362–6370, Aug. 2017.
[24] W. Li, X. Ruan, D. Pan, and X. Wang, "Full-feedforward schemes of grid voltages for a three-phase *LCL*-type grid-connected inverter," *IEEE Trans. Ind. Electron.*, vol. 60, no. 6, pp. 2237–2250, Jun. 2013.
[25] Y. Gu, Y. Wang, X. Xiang, W. Li, and X. He, "Improved virtual vector control of single-phase inverter based on unified model," *IEEE Trans. Energy Convers.*, vol. 29, no. 3, pp. 611–618, Sep. 2014.
[26] J. Ma, X. Wang, F. Blaabjerg, L. Harnefors, and W. Song, "Accuracy analysis of the zero-order hold model for digital pulse width modulation," *IEEE Trans. Power Electron.*, vol. 33, no. 12, pp. 10826–10834, Dec. 2018.
[27] B. Wen, D. Boroyevich, R. Burgos, P. Mattavelli, and Z. Shen, "Analysis of D-Q small-signal impedance of grid-tied inverters," *IEEE Trans. Power Electron.*, vol. 31, no. 1, pp. 675–687, Jan. 2016.
[28] Y. Gu, J. Liu, T. Green, W. Li, and X. He, "Motion-induction compensation to mitigate sub-synchronous oscillation in wind farms," *IEEE Trans. Sustain. Energy*, to be published, doi: 10.1109/TSTE.2019.2921662.
[29] B. Wen, R. Burgos, D. Boroyevich, P. Mattavelli, and Z. Shen, "AC stability analysis and dq frame impedance specifications in power-electronics-based distributed power systems," *IEEE J. Emerg. Sel. Topics Power Electron.*, vol. 5, no. 4, pp. 1455–1465, Dec. 2017.
[30] J. Sun, "Impedance-based stability criterion for grid-connected inverters," *IEEE Trans. Power Electron.*, vol. 26, no. 11, pp. 3075–3078, Nov. 2011.
[31] Y. Han, M. Yang, H. Li, P. Yang, L. Xu, E. A. A. Coelho, and J. M. Guerrero, "Modeling and stability analysis of *LCL*-type grid-connected inverters: A comprehensive overview," *IEEE Access*, vol. 7, pp. 114975–115001, 2019.
[32] Y. Lei, W. Xu, C. Mu, Z. Zhao, H. Li, and Z. Li, "New hybrid damping strategy for grid-connected photovoltaic inverter with LCL filter," *IEEE Trans. Appl. Supercond.*, vol. 24, no. 5, Oct. 2014, Art. no. 0601608.
[33] R. Peña-Alzola, M. Liserre, F. Blaabjerg, R. Sebastián, J. Dannehl, and F. W. Fuchs, "Analysis of the passive damping losses in LCL-filter-based grid converters," *IEEE Trans. Power Electron.*, vol. 28, no. 6, pp. 2642–2646, Jun. 2013.
[34] W. Li, "Research on suppressing harmonic and unbalanced injected grid currents caused by grid voltages for the three-phase LCL-type grid-connected inverter," Ph.D. dissertation, School Elect. Electron. Eng., Huazhong Univ. Sci. Technol., Wuhan, China, Apr. 2014.

HUAIYUAN LIU received the B.S. degree in electrical engineering from the Harbin Institute of Technology, Harbin, China, in 2013, where he is currently pursuing the Ph.D. degree. His current area of interest is stability analysis and control of power converters in renewable energy generation systems.

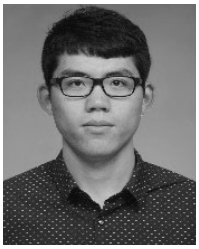

LEI LI received the B.S. and M.S. degrees in electrical engineering from the Harbin Institute of Technology, Harbin, China, in 2014 and 2019, respectively, where he is currently pursuing the Ph.D. degree. His current areas of interests are the power quality improvement and high power DC/DC converters.

YUCHAO LIU received the B.S. degree in electronic information engineering from the Harbin University of Science and Technology, Harbin, China, in 2011, and the M.S. and Ph.D. degrees in electrical engineering from the Harbin Institute of Technology, Harbin, in 2014 and 2019, respectively. From 2017 to 2018, she had been a Visiting Student with Imperial College London, U.K. She is currently a Lecturer with the College of Automation, Harbin Engineering University. Her area of interest is the control strategy and stability analysis of multiterminal DC transmission.

DIANGUO XU (M'97–SM'12–F'17) received the B.S. degree in control engineering from Harbin Engineering University, Harbin, China, in 1982, and the M.S. and Ph.D. degrees in electrical engineering from the Harbin Institute of Technology (HIT), Harbin, China, in 1984 and 1989, respectively. In 1984, he joined the Department of Electrical Engineering, HIT, as an Assistant Professor, where he has been a Professor at the Department of Electrical Engineering, since 1994. He was the Dean of the School of Electrical Engineering and Automation, HIT, from 2000 to 2010. He was the Assistant President of the HIT, from 2010 to 2014, where he is currently the Vice President. He has authored or coauthored four books and published over 600 technical articles. He holds 54 Chinese patents. His research interests include renewable energy generation technology, M-VSC-HVDC transmission systems, power quality mitigation, and speed sensorless vector controlled motor drives. He serves as the Chairman of the IEEE Harbin Section. He is an Associate Editor for the IEEE TRANSACTIONS ON INDUSTRIAL ELECTRONICS.

QIANG GAO received the B.S., M.S., and Ph.D. degrees in electrical engineering from the Harbin Institute of Technology, Harbin, China, in 1986, 2004, and 2009, respectively. In 2004, he joined the Department of Electrical Engineering, Harbin Institute of Technology, as a Professor, where he has been the Director of the Department of Electrical Engineering, Institute of Power Electronics and Electrical Drives, since 2011. His current research interests include high-power ac motor drives, high-temperature power electronics, and smart well and digital oil field.